Synthesis, Structure, and Physical Properties of $Nb_{18}P_{2.5}O_{50}$

J. Xu, S. C. Chen, K. V. Ramanujachary, and M. Greenblatt*

Department of Chemistry, Rutgers, The State University of New Jersey, Piscataway, New Jersey 08855-0939

Received September 10, 1992®

The crystal structure of a new niobium phosphate bronze, $Nb_{18}P_{2.5}O_{50}$, was determined by single-crystal X-ray diffraction, and its physical properties were studied. $Nb_{18}P_{2.5}O_{50}$ crystallizes in the tetragonal system with space group $I4/m$ (No. 87) and $Z = 1$. The unit cell parameters are $a = 15.593(1)$ Å, $c = 3.8282(3)$ Å, and $V = 930.8(1)$ Å^3. The structural refinement by a full-matrix least-squares technique led to $R = 0.055$ ($R_w = 0.052$). The structure of $Nb_{18}P_{2.5}O_{50}$ is built up from 3 × 3 slabs of ReO_3-type NbO_6 octahedra. These slabs are stacked alternatively along the crystallographic c axis and joined together by edge-sharing. In the ab plane, the slabs of NbO_6 octahedra are interconnected through corner-sharing PO_4 tetrahedra. Single-crystal resistivity measurement of $Nb_{18}P_{2.5}O_{50}$ along the crystallographic c axis showed a semiconducting behavior with an activation energy of 0.13(1) eV. The magnetic susceptibility data indicate a modified Curie–Weiss behavior with the Curie–Weiss temperature $\Theta = -3.70$ K and $\mu_{eff}/Nb^{4+} = 0.8\ \mu_B$.

Introduction

The structure of the high-temperature form of Nb_2O_5[1] is built up of ReO_3-type slabs of 3 × 4 and 3 × 5 corner-sharing NbO_6 octahedra, which are connected by NbO_4 tetrahedra to form layers. The layers are stacked in the third direction by edge sharing of NbO_6 octahedra to form a three-dimensional (3D) network structure. The structure of Nb_9PO_{25},[2] characterized by Roth *et al.*, is related to the high-temperature form of Nb_2O_5; however, in Nb_9PO_{25}, the 3 × 3 slabs of corner-sharing NbO_6 octahedra in the ab plane of the tetragonal structure are connected by PO_4 tetrahedra, rather than NbO_4 tetrahedra. The layers are arranged in the c crystallographic direction by edge-sharing of NbO_6 octahedra as in Nb_2O_5. The arrangement of corner-/edge-sharing polyhedra creates a structure which may be represented by the formula $^oNb_9{}^tP_xO_{25}$ with $1 \le x \le 2$; i.e., it is nonstoichiometric in P (where o and t represent octahedral and tetrahedral sites, respectively). Thus in Nb_9PO_{25} the tetrahedral sites are only 50% occupied by P. With an increase in the occupancy of the tetrahedral sites by phosphorus ($x > 1$), the oxidation state of niobium is lowered and the 4d orbitals of Nb are no longer empty. Further, since the PO_4 tetrahedra are insulating, while the NbO_6 slabs may become conducting if the d electrons delocalize over the NbO_6 slabs, quasi-low-dimensional properties might be observed. We report here the synthesis, crystal structure, and physical properties of a new reduced niobium phosphate bronze, $Nb_{18}P_{2.5}O_{50}$, which is isostructural with Nb_9PO_{25}.

Experimental Section

Synthesis. Large single crystals of $Nb_{18}P_{2.5}O_{50}$ were obtained in a reaction which was intended to grow single crystals of $Na_3BaNb_8P_4O_{32}$.[3] The largest crystal grown has approximate dimensions of 1.0 × 1.2 × 2.0 mm^3. The synthetic procedure was performed in two steps. A reaction mixture containing Na_2CO_3 (Fisher, ACS Certified grade), $BaCO_3$ (Johnson Matthey, 99.9%), Nb_2O_5 (Alfa, 99.5%), and $(NH_4)_2HPO_4$ (Fisher, 99.7%) in a molar ratio of 1.5:1:3.9:4 was ground in an agate mortar and heated at 650 °C in a porcelain crucible overnight to remove CO_2, H_2O, and NH_3. The resulting powder was then mixed with an adequate amount of niobium metal powder (Johnson Matthey Electronics, 99.8%) to achieve a composition of $Na_3BaNb_8P_4O_{32}$ and was pelletized and sealed in an evacuated quartz tube. The quartz tube was horizontally placed inside a muffle furnace and heated at 1150 °C for 20 days. The reaction vessel was slowly cooled (5 °C/h) to 500 °C, and the reaction was then quenched at room temperature in air. The well-formed prismatic crystals were washed with 10% (in weight) HF at 50 °C. Single-crystal growth from a stoichiometric mixture of $Nb_{18}P_{2.5}O_{50}$ was also tried, but only tiny crystals (about 0.01 × 0.03 × 0.05 mm^3) were obtained.

The polycrystalline powder of $Nb_{18}P_{2.5}O_{50}$ was prepared from stoichiometric mixtures of $(NH_4)_2HPO_4$ and Nb_2O_5 to obtain the composition $Nb_{17.5}P_{2.5}O_{50}$. This mixture was ground intimately and heated at 400 °C for 20 h with two intermittent grindings to ensure a complete decomposition of $(NH_4)_2HPO_4$. The resulting powder was mixed with an appropriate amount of Nb powder and then pelletized, sealed in an evacuated quartz tube and heated at 1000 °C for 10 hours. In this way, dark blue polycrystalline $Nb_{18}P_{2.5}O_{50}$ was obtained.

Single-Crystal X-ray Crystallographic Study. A prismatic crystal having approximate dimensions of 0.12 × 0.15 × 0.36 mm^3 was chosen for single-crystal study. Data were collected with an Enraf-Nonius CAD-4 diffractometer at room temperature. Lattice parameters and the orientation matrix for data collection were measured from 25 carefully centered reflections in the range $13° < 2\theta < 32°$. Graphite-monochromatized Mo Kα radiation was employed to collect data with $4° \le 2\theta \le 50°$. A scan mode of ω–2θ was used. Three standard reflections showed no apparent variation in intensity during the data collection. The linear absorption coefficient for Mo Kα is 54.0 cm^{-1}. An empirical absorption correction was applied, based on azimuthal scans of three reflections with transmission factors in the range from 0.3858 to 0.9415. The intensity data were corrected for Lorentz and polarization effects. A correction for secondary extinction was also applied. Data collected in the quadrant $(h,k,\pm l)$ were averaged to give a total of 898 reflections of which 479 reflections with $I > 3\sigma(I)$ were considered as observed. The space group ($I4/m$) was chosen on the basis of the statistical analysis of intensity distribution and systematic absences of hkl ($h + k + l \neq 2n$), $hk0$ ($h + k \neq 2n$), $0kl$ ($k + l \neq 2n$), hhl ($l \neq 2n$), $00l$ ($l \neq 2n$), and $0k0$ ($k \neq 2n$). The structure was solved by direct methods (SHELXS-86)[4] and refined on $|F|$ by a full-matrix least-squares technique in the MoLEN program package.[5] A θ-dependent absorption correction following the DIFABS procedure[6] was applied to the isotropically refined structure. The minimum and maximum correction factors were 0.6211 and 1.1162, respectively. At this stage of the refinement, the isotropic temperature factor for the P atom was 3.93 Å^2. The occupancy refinement was thus

* To whom correspondence should be addressed.

® Abstract published in *Advance ACS Abstracts*, December 15, 1993.

(1) Gatehouse, B. M.; Wadsley, A. D. *Acta Crystallogr.* **1964**, *17*, 1545.
(2) Roth, R. S.; Wadsley, A. D.; Anderson, S. *Acta Crystallogr.* **1965**, *18*, 643.
(3) Costentin, G.; Borel, M. M.; Grandin, A.; Leclaire, A.; Raveau, B. *Mater. Res. Bull.* **1991**, *26*, 1051.
(4) Sheldrick, G. M., Krager, C., Goddard, R., Eds. *Crystallographic Computing 3*; Oxford University Press: Oxford, U.K., 1985; pp 175–189.
(5) Fair, C. K. *MoLEN*; Enraf-Nonius, Delft Instruments X-Ray Diffraction BV: Rontgenweg 1, 2624BD Delft, The Netherlands, 1990.
(6) Walker, N.; Stuart, D. *Acta Crystallogr.* **1983**, *A39*, 158.

0020-1669/94/1333-0267$04.50/0

Table 1. X-ray Crystallographic Data for $Nb_{18}P_{2.5}O_{50}$

fw	2549.72	ρ_{calcd} (g/cm^3)	4.549
space group	$I4/m$ (No. 87)	μ(Mo Kα) (cm^{-1})	54.0
a (Å)	15.593(1)	λ (Å), graphite-monochromated	0.710 69
c (Å)	3.8282(3)		
V (Å^3)	930.8(1)	R^a	0.055
Z	1	R_w^b	0.052
t (°C)	20		

$^a R = \sum\|F_o| - |F_c\|/\sum|F_o|$. $^b R_w = [\sum w(|F_o| - |F_c|)^2/\sum w|F_o|^2]^{1/2}$; $w = (\sigma^2|F_o|)^{-1}$.

Table 2. Atomic Coordinates and B_{eq} Values for $Nb_{18}P_{2.5}O_{50}$

atom	x	y	z	$B_{eq}{}^a$ (Å^2)
Nb(1)	0.000	0.000	0.000	1.55(5)
Nb(2)	0.21843(8)	0.10890(8)	0.000	0.40(2)
Nb(3)	0.11428(8)	0.32977(8)	0.000	0.45(2)
P^b	0.000	0.500	0.25	1.5(1)
O(1)	0.1751(6)	0.2203(6)	0.000	2.2(2)
O(2)	0.2820(7)	0.9885(6)	0.000	2.1(2)
C(3)	0.2472(6)	0.3893(7)	0.000	1.8(2)
O(4)	0.3543(6)	0.1561(7)	0.000	2.1(2)
O(5)	0.0664(7)	0.4512(7)	0.000	2.3(2)
O(6)	0.1169(6)	0.0518(7)	0.000	1.9(2)
O(7)	0.500	0.500	0.000	3.0(4)

$^a B_{eq} = 8\pi^2/3\sum U_{ij}a_i^*a_j^*\mathbf{a}_i\cdot\mathbf{a}_j$, where the temperature factors are defined as $\exp(-2\pi^2\sum h_ih_ja_i^*a_j^*U_{ij})$. ^{b} P partially occupies the 4d position with 62.5% occupancy in the $I4/m$ (No. 87) space group.

Table 3. Selected Bond Distances (Å) for $Nb_{18}P_{2.5}O_{50}$

Nb(1)–O(6) (×4)	1.995(9)	Nb(3)–O(1)	1.95(1)
Nb(1)–O(7) (×2)	1.914(0)	Nb(3)–O(2)	1.77(1)
Nb(2)–O(1)	1.86(1)	Nb(3)–O(3)	2.27(1)
Nb(2)–O(2)	2.12(1)	Nb(3)–O(4) (×2)	1.988(3)
Nb(2)–O(3) (×2)	1.988(3)	Nb(3)–O(5)	2.04(1)
Nb(2)–O(4)	2.24(1)	P–O(5) (×4)	1.603(8)
Nb(2)–O(6)	1.82(1)		

applied to the P atom before the structure was refined anisotropically. The structure based on 479 observed reflections and 57 variable parameters was then anisotropically refined to $R = 0.055$ and $R_w = 0.052$. The final electron density map was flat with a maximum peak of 2.93 e/Å^3 close to Nb(1) and a minimum of −2.355 e/Å^3 located at (0.2673, 0.0417, 0.0020).

Selected X-ray crystallographic data for $Nb_{18}P_{2.5}O_{50}$ are given in Table 1. Final positional parameters are listed in Table 2, and the corresponding selected bond distances are presented in Table 3.

Physical Property Measurements. A single crystal of $Nb_{18}P_{2.5}O_{50}$ with a length of approximately 2 mm was used for the electrical resistivity measurements along the crystallographic c axis; a standard four-probe technique with a Displex cryostat (APD Cryogenics, DE-202) in the temperature range 20–300 K was employed. The orientation of the crystallographic c axis was determined by oscillation photographs, and ohmic contacts to the crystal were made by attaching molten indium ultrasonically. The magnetic susceptibility measurements were carried out on a batch of randomly oriented single crystals (0.0168 g) with a Quantum Design SQUID magnetometer in the temperature range 2–300 K. The magnetic field applied was 0.5 T.

Results and Discussion

The composition, $Nb_{18}P_{2.5}O_{50}$, was derived from the structural refinement, which indicated an occupancy of 0.625 for P.

Description of Structure. $Nb_{18}P_{2.5}O_{50}$ is isostructural with Nb_9PO_{25} studied by Roth *et al.*[2] However, the structural solution of the latter compound was derived from Weissenberg photographs with an undetermined space group. As shown in Figure 1, the structure of $Nb_{18}P_{2.5}O_{50}$ is built up from corner-sharing NbO_6 octahedra and PO_4 tetrahedra. Nine NbO_6 octahedra corner-share to form a 3 × 3 slab in the ab plane. These slabs are oriented along the [520] direction and are held together by corner-sharing PO_4 tetrahedra. The three-dimensional structure, illustrated in Figure 2, is built up of the layers shown in Figure 1 stacked along the crystallographic c axis with shifts of $0.5a$, $0.5b$, and $0.5c$. The NbO_6 octahedra between the layers are edge-shared. Three different types of tunnels are thus created along the c axis: a perovskite tunnel formed by one Nb(1)O_6, two Nb(2)O_6, and one Nb(3)O_6 octahedra from the same layer (Figure 1); a four-sided tunnel formed by two Nb(2)O_6 and two Nb(3)O_6 from different layers (Figure 2); and a distorted four-sided tunnel formed by one Nb(2)O_6, two Nb(3)O_6, and one PO_4 from different layers (Figure 2).

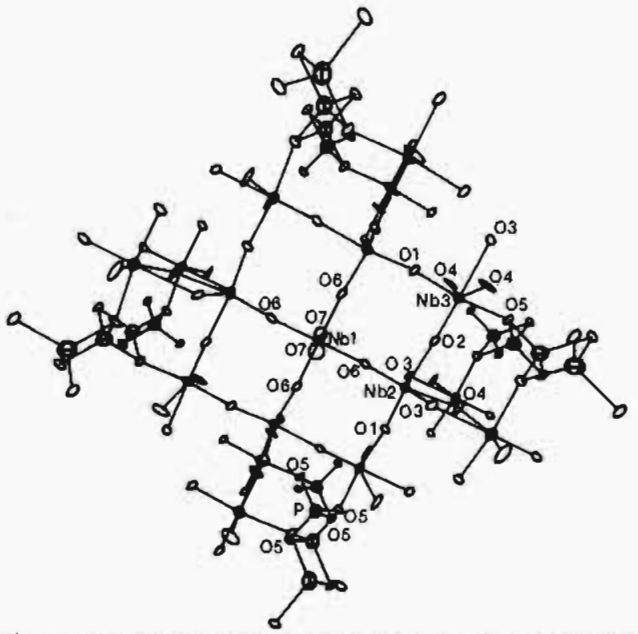

Figure 1. ORTEP drawing (74% thermal ellipsoids) of the $Nb_{18}P_{2.5}O_{50}$ structure showing the 3 × 3 slab of corner-sharing NbO_6 octahedra and PO_4 tetrahedra in the ab plane at $z = 0.0$.

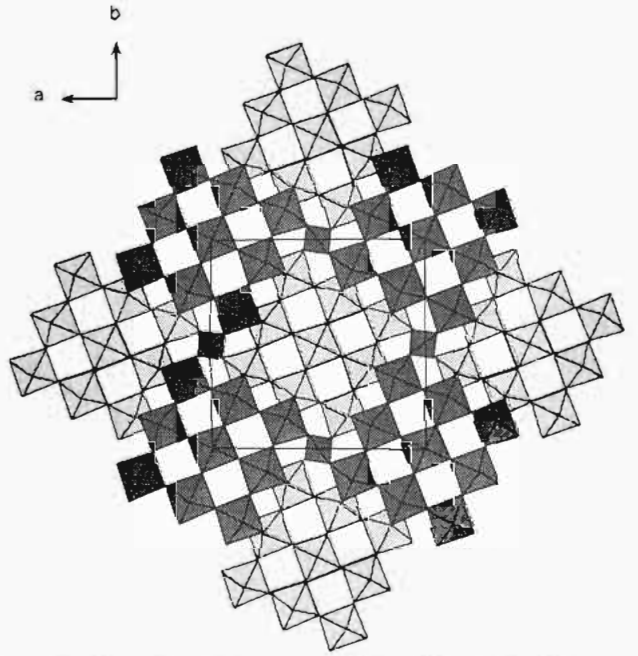

Figure 2. Projection of the structure of $Nb_{18}P_{2.5}O_{50}$ in the ab plane.

There are three unique NbO_6 octahedra and one PO_4 tetrahedron in $Nb_{18}P_{2.5}O_{50}$. The Nb(1)O_6 octahedron is corner-shared with four Nb(2)O_6 octahedra in the ab plane and two Nb(1)O_6 octahedra along the c axis. The Nb(2)O_6 is corner-shared with one Nb(1)O_6, two Nb(3)O_6 in the ab-plane, and two Nb(2)O_6 along the c axis and cis-edge-shared with two Nb(3)O_6 along the c axis. The Nb(3)O_6 octahedra are corner-shared with two Nb(2)O_6 and one PO_4 in the ab plane and two Nb(3)O_6 along the

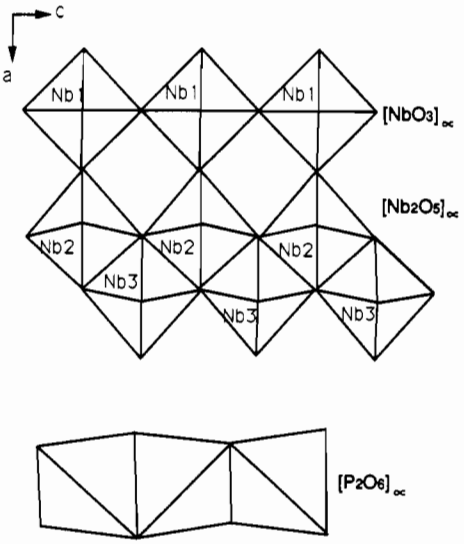

Figure 3. Three types of infinite chains of polyhedra present along the c axis in $Nb_{18}P_{2.5}O_{50}$.

c axis and are cis-edge-shared with two $Nb(2)O_6$ along the c axis. The PO_4 tetrahedra are corner-shared with four $Nb(3)O_6$ from two different layers in the ab plane and edge-shared with two PO_4 along the c axis. Three types of infinite chains of polyhedra running along the c axis are observed in the structure of $Nb_{18}P_{2.5}O_{50}$ (Figure 3). The corner-sharing $Nb(1)O_6$ octahedra along the c axis form the linear chains of $[NbO_3]_\infty$. The cis-edge-shared $Nb(2)O_6$ and $Nb(3)O_6$ octahedra along the c axis lead to the zigzag chains of $[Nb_2O_5]_\infty$, which are oriented along either the [120] or [$\bar{2}$10] direction. The edge-sharing PO_4 tetrahedra form the linear chain of $[P_2O_6]_\infty$ along the c axis. These infinite chains of polyhedra are held together through corner-sharing in the ab plane.

As shown in Table 3, the Nb–O bond distances range from 2.27(1) Å for Nb(3)–O(3) to 1.77(1) Å for Nb(3)–O(2); these bonds are highly distorted in order to reduce the structural strains created by the edge-sharing octahedra. The unusual long bond distances of Nb(3)–O(3) and Nb(2)–O(4) (2.24(1) Å) most likely arise from the higher coordination number (CN = 3) around the O(3) and O(4) atoms, which results from edge-sharing between the $Nb(2)O_6$ and $Nb(3)O_6$ octahedra. In addition, the unusually short bond distance of Nb(3)–O(2) and the long distance of Nb(2)–O(2) (2.12(1) Å), as compared with the average Nb–O bond distances of 1.992 Å in $Nb_{18}P_{2.5}O_{50}$, occur to reduce the strains due to the edge-sharing of octahedra. The Nb(2) and Nb(3) atoms are pushed away from O(4) and O(3), respectively, to reduce the electrostatic repulsion between Nb atoms from different layers (Figure 2). The relatively long distance (2.04(1) Å) of Nb(3)–O(5), as compared to that of Nb(3)–O(1) (1.95(1) Å), is consistent with the covalent character of the P–O bond and agrees well with the general observation in niobium phosphate bronzes that the Nb–O distances involving oxygen atoms common to one Nb and one P atom are generally longer than those involving oxygen atoms common to two Nb atoms.[7-11] The $Nb(1)O_6$ octahedron is in the center of a 3 × 3 array of octahedra and is slightly distorted from octahedral to tetragonal geometry with the tetragonality ratio $c/a \leq 1$. This relatively small distortion

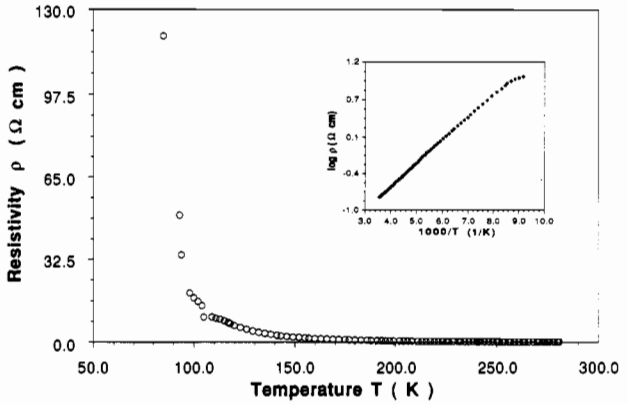

Figure 4. Resistivity as a function of temperature along the c axis of a single crystal of $Nb_{18}P_{2.5}O_{50}$. The inset is the plot of log ρ vs $1/T$ in the temperature range 120–300 K.

of $Nb(1)O_6$ octahedra, as compared to those of $Nb(2)O_6$ and $Nb(3)O_6$ octahedra, is likely due to the relatively small strains due to the corner-sharing of $Nb(1)O_6$ with $Nb(2)O_6$, as compared with that due to the cis-edge-sharing of $Nb(2)O_6$ and $Nb(3)O_6$ in two different layers.

The P–O distance of 1.603(8) Å is significantly longer than the characteristic P–O distance of 1.55 Å in monophosphate groups but close to those observed in the NbO_4 tetrahedra belonging to the high-temperature form of Nb_2O_5.[1]

Electrical Resistivity. Figure 4 shows electrical resistivity data of a $Nb_{18}P_{2.5}O_{50}$ single crystal measured along the crystallographic c axis in the temperature range 20–300 K. The resistivity along the c axis at room temperature is 0.16 Ω cm and increases exponentially with decreasing temperature, indicating semiconducting behavior. The thermal activation energy (E_a) for conduction estimated from the linear portion of the plot of log ρ vs $1/T$ (inset in Figure 4) in the temperature range 120–300 K is 0.13 (±0.01) eV. The room-temperature resistivity along the direction perpendicular to the crystallographic c axis is approximately 2 orders of magnitude larger than that along the c axis. These results are consistent with the structural arrangement of NbO_6 and PO_4 polyhedra discussed earlier. Along the c axis, the arrangement of NbO_6 octahedra favors the formation of a wide conduction band; thus electron delocalization along the c axis is expected. Moreover, the connection between NbO_6 octahedra and PO_4 tetrahedra in the ab plane could result in higher resistivity. The semiconducting behavior observed along the c axis of $Nb_{18}P_{2.5}O_{50}$ is somewhat surprising, considering the columns of mixed-valent 3 × 3 × ∞ NbO_6 octahedra. Recently, Cava *et al.* reported the electrical and magnetic properties of $Nb_2O_{5-\delta}$ ($0 \leq \delta \leq 0.16$).[12] The electrical resistivity of these compounds changes from semiconducting to metallic with increasing δ which has been attributed to the increased electron density induced by oxygen deficiency. For metallic $Nb_2O_{5-\delta}$, δ is ~0.16, corresponding to a critical value of ~16.6% Nb^{4+} per formula. In $Nb_{18}P_{2.5}O_{50}$, the Nb^{4+} content is 13.9% per formula, which appears to be smaller than that required for metallic conduction. Furthermore, the semiconducting behavior of $Nb_{18}P_{2.5}O_{50}$ can also be attributed to the local distortion of NbO_6 octahedra, which would hinder the motion of electrons through the lattice.

Magnetic Susceptibility. The temperature-dependent molar magnetic susceptibility of $Nb_{18}P_{2.5}O_{50}$ corrected for the core diamagnetism of component ions is presented in Figure 5. The susceptibility remains nearly temperature independent in the range 100–300 K; however the presence of localized moments is evident from the upturn in the susceptibility seen below 100 K (Figure 5). The magnetic susceptibility in the temperature range 2–200

(7) Leclaire, A.; Benabbas, A.; Borel, M. M.; Grandin, A.; Raveau, B. *J. Solid State Chem.* **1989**, *83*, 245.
(8) Costentin, G.; Borel, M. M.; Grandin, A.; Leclaire, A.; Raveau, B. *J. Solid State Chem.* **1991**, *90*, 279.
(9) Benabbas, A.; Borel, M. M.; Grandin, A.; Leclaire, A.; Raveau, B. *J. Solid State Chem.* **1991**, *95*, 245.
(10) Benabbas, A.; Borel, M. M.; Grandin, A.; Leclaire, A.; Raveau, B. *J. Solid State Chem.* **1991**, *92*, 51.
(11) Borel, M. M.; Goreaud, M.; Grandin, A.; Labbe, Ph.; Leclaire, A.; Raveau, B. *Eur. J. Solid State Inorg. Chem.* **1991**, *28*, 93 and references therein.
(12) Cava, R. J.; Botlogg, B.; Krajewski, J. J.; Poulsen, H. F.; Gammel, P.; Peck, W. F.; Rupp, L. W., Jr. *Phys. Rev. B* **1991**, *44*, 6973.

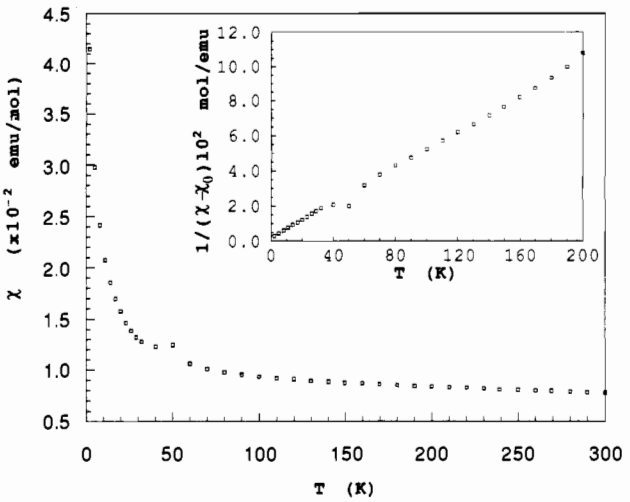

Figure 5. Temperature-dependent molar magnetic susceptibility for a batch of randomly oriented single crystals. Inset shows the plot of $1/(\chi - \chi_0)$ vs temperature.

K could be fit to a modified Curie–Weiss relation according to the following equation:

$$\chi = \chi_0 + C/(T - \Theta)$$

where, χ_0 = temperature-independent contributions such as Van Vleck and Pauli magnetism, C = Curie constant, and Θ = Curie–Weiss temperature. A nonlinear least-squares fitting of the observed data yielded $\chi_0 = 7.5 \times 10^{-3}$ emu/mol, $C = 0.19(1)$ emu K/mol, and $\Theta = -3.7$ K. A plot of $1/(\chi - \chi_0)$ as a function of temperature is nearly linear in the range 2–200 K (inset of Figure 5). A small anomaly seen at ~50 K arises from the antiferromagnetic ordering of absorbed O_2.[13] Deviations from linearity, evident in the data above 200 K, presumably are due to the low susceptibility of the sample at these temperatures as has been reported by Raveau and co-workers regarding the magnetic properties of various phosphate niobium bronzes.[14] Alternatively, the deviations in χ at higher temperatures might also arise from the simultaneous operation of more than one type of Curie–Weiss relation such as $\chi = \chi_0 + C/(T - \Theta) + C'/(T - \Theta')$. Here C and C' are the Curie constants associated with two different types of paramagnetic centers. However, the ambiguity in locating the Nb^{4+} centers precisely in the structure has precluded us from further analysis of this possibility.

From valence considerations, the presence of local moments can be attributed to the $4d^1$ electrons associated with the Nb^{4+} centers in the structure. The effective magnetic moment (μ_{eff}), estimated from the relationship $\chi = N\beta^2\mu_{eff}^2/3k_BT$ (where N is Avagadro's number, k_B is the Boltzmann constant, and β is the Bohr magnetron), is 0.80 μ_B/Nb^{4+}, which is considerably smaller than the expected value of 1.73 μ_B based on the spin-only contributions of $4d^1$ electrons. This difference in the observed and theoretical effective magnetic moments implies that only a fraction of the charge carriers are localized, while the remaining must be delocalized, giving rise to the observed conductivity. In fact, the observed effective magnetic moment (0.80 μ_B/Nb^{4+}) is in excellent agreement with the corresponding values reported for the $Nb_2O_{5-\delta}$ system.[14] Finally, the small negative Weiss temperature ($\Theta = -3.7$ K) is indicative of very weak antiferromagnetic correlations between the localized moments.

Conclusions

We have synthesized and characterized a new reduced niobium phosphate bronze, $Nb_{18}P_{2.5}O_{50}$, which is structurally related to the high-temperature form of Nb_2O_5[1] and is isostructural with Nb_9PO_{25}.[2] Both $Nb_{18}P_{2.5}O_{50}$ and Nb_9PO_{25} have a partial occupancy of the phosphorus atoms in the tetrahedral sites. The electrical transport and the magnetic properties of these compounds may be tuned by variation of the partial occupancy in the tetrahedral site. For example, Nb_9PO_{25} is white and insulating, while $Nb_{18}P_{2.5}O_{50}$ is dark blue and semiconducting. With more phosphorus content, it is likely that a quasi-low-dimensional metallic niobium phosphate bronze can be obtained. To better understand how the physical properties of $Nb_{18}P_xO_{50}$ ($2 \leq x \leq 4$) vary with the phosphorus content, we are currently in the process of preparing the analogous compounds with $x = 3.0$, 3.5, and 4.0.

Acknowledgment. We thank Z. Zhang for helping with the resistivity measurement and Z. Teweldemedhin for helping with the magnetic susceptibility measurement. This work was supported by the National Science Foundation—Solid State Chemistry Program (Grant DMR-90-19301).

Supplementary Material Available: Tables giving X-ray crystallographic details, bond lengths, bond angles, anisotropic thermal parameters, and powder X-ray diffraction data (6 pages). Ordering information is given on any current masthead page.

(13) Quantum Design Technical Advisory MPMS No. 8, Quantum Design, Inc., 1990.
(14) Benabbas, A.; Provost, J.; Borel, M. M.; Leclaire, A.; Raveau, B. *Chem. Mater.* **1993**, *5*, 1143.